Modelling of Electrically-Assisted Turbocharger Compressor Performance

Mamdouh Alshammari[1], Nikolaos Xypolitas[1], Apostolos Pesyridis[1]

[1] College of Engineering and Design, Brunel University London, Uxbridge, UB8, UK; Mamdouh.Alshammari@brunel.ac.uk; 1613912@brunel.ac.uk

* Correspondence: a.pesyridis@brunel.ac.uk; Tel.: +44-1895-267-901

Abstract: For the purposes of design of a turbocharger centrifugal compressor, a one-dimensional modelling method has been developed and applied specifically to electrically-assisted turbochargers (EAT). For this purpose, a mix of authoritative loss models was applied to determine the compressor losses. Furthermore, an engine equipped with an electrically-assisted turbocharger was modelled using commercial engine simulation software (GT-Power) to assess the performance of the engine equipped with the designed compressor. A commercial 1.5L gasoline, in-line, 3-cylinder engine was selected to be modelled. In addition, the simulations have been performed for an engine speed range of between1000 and 5000 rpm. The design target was an electric turbocharger compressor that could meet the boosting requirements of the engine with noticeable improvement in transient response. The results from the simulations indicated that the EAT improved the overall performance of the engine compared to the equivalent conventional turbocharged engine model. Moreover, the electrically-assisted turbochargers (EAT) equipped engine with power outputs of 1kW and 5kW EAT was increased by an average of 5.96% and 15.4%, respectively, ranging from 1000 rpm to 3000 rpm engine speed. For the EAT model of 1kW and 5kW, the overall net reduction of the BSFC was 0.53% and 1.45%, respectively from the initial baseline engine model.

Keywords: Centrifugal compressor; electrically-assisted turbocharger; 1D modelling; compressor design; transient response.

1. Introduction

1.1 General Turbocharging Advantages and Limitations

The impact of global warming has forced regulatory authorities around the world to establish strict regulations on CO_2 emissions and other greenhouse gas emissions. Although the regulations created several technical challenges for automotive industry, this led to technology development as there was a demand of decreasing the fuel consumption of engines, increasing their performance as result more power and more sustainable products had to be designed to reduce their environmental impact [1-3]. Among various technologies that have been developed, the most effective way to increase the fuel economy and decrease the CO_2 emissions of passenger vehicles is engine downsizing[4][5]. The purpose of engine downsizing is the reduction of the throttling and friction losses associated with a larger engine by using a smaller, high power-density engine. Thus, the engine efficiency is improved by operating in the more efficient regions, with the boosting device (turbocharger or supercharger) being the crucial component that allows this significantly increased power density to occur.

However, these conventional boosting devices have some limitations. Traditionally, the main drawback of the turbocharger is the delay in generating boost pressure which results in insufficient torque at low engine speeds, known as turbo lag [1][6]. Conversely, the mechanical supercharger has a fast response at low engine speed, but it creates parasitic losses to the engine as the required power for its operation is taken from the engine. One feasible solution for avoiding the drawbacks of the conventional boosting technologies is the electrification of the boosting system [7] [8]. Not only do electrification systems reduce the transient response (turbo lag) by 50-400% with respect to time-to-torque depending on the operating point of the turbocharger and engine, but they can also increase the overall engine efficiency for a substantial part of the turbocharged-engine operating range when compared to equivalent mechanical turbocharger systems [9][10]. Therefore, the aim of the paper is to model an advanced electric turbocharger compressor to improve the transient response of the turbocharger at low engine speed and in turn to enhance the performance, efficiency and fuel economy of the engine.

1.2 Electrically Assisted Turbocharger (EAT)

Katrasnik et al. [11] evaluated the electrical assisted turbocharger in which the torque is applied to the turbocharger using a high speed electric motor. The motor can be integrated into the turbocharger bearing housing, or as an extension to the turbocharger shaft on the compressor side. On the other hand, Baines [12] claimed this type of arrangement would be a less severe working environment for the motor than that of electrically driven compressor in a combined charging system. However, the unit size will be increased and the effects on the shaft dynamics could be problematic. Generally, more weight will be added by the motor, thus, it will affect bearing loads, and also will increase the base inertia of the turbocharger. Nonetheless, the motor can be operated as generator to recover the exhaust energy as electric power which is an additional feature. Katrasnik et al. [11] conducted an experiment in which the transient response and load acceptance of a 6.9L 6 cylinder commercial diesel engine were simulated with the original fixed geometry turbocharger installed and also with two electrically assisted variants. After collaborating and validating the engine model with the experiment data, the transient response of the engine at a fixed speed tip-in was decreased by up to 55% with an electrically assisted turbocharger, the acceptance load was considerably developed.

1.3 Preliminary Design of Centrifugal Compressors

Yang et al [7] developed a radial compressor for an electric supercharger in a 2.0L petrol engine by using a mean-line design process. In the process, the operating conditions of the compressor were provided and a set of geometrical parameters were selected to start the design. Then, computational fluid dynamics (CFD) simulation was applied in a detailed 3D design to analyse the compressor's performance. The results of computational fluid dynamics (CFD) simulation method showed a moderate reduction in total pressure ratio and total impeller efficiency compared to the predicted corresponding values in the meanline method. However, it is worth noting that the scroll was excluded in the computational fluid dynamics (CFD) simulation, hence in this method, the predicted values of total pressure ratio and total efficiency were slightly increased as the scroll loss was not included. Therefore, there is a significant difference in the results obtained from 1D modelling method and the computational fluid dynamics (CFD) simulation.

On the other hand, Harley et al [13] developed a novel meanline modelling method for radial compressors that is applied in automotive turbochargers. In this modelling approach, the pressure ratio and the recirculation flow of the compressor are linked. Furthermore, Harley et al [13] stated that the results obtained from the existing meanline methods would not be accurate in comparison with test data as the pressure ratio is predicted and thus it could rise and lead to surge. However, the new method deals with the issue by modelling the recirculation effects. Three different diameter centrifugal compressors with vaneless diffusers and scroll collectors were used for the process [13]. The procedure starts with the analysis of the inlet blockage creation by recirculation flow and how this affects the induced flow into the impeller. Galvas [14] loss model collection was selected for the analysis as according to Harley et al [13][15][16] not only is a robust model, but it also operates best across a variety of automotive turbocharger radial designs. Then, computational fluid dynamics (CFD) modelling was applied to verify all the results. The results indicate that with the proposed meanline modelling process, the prediction methods are improved as the flow conditions are represented more accurately in the impeller. A major positive outcome of this study is that the novel method could be used for any centrifugal compressor to improve the blade angle selection when recirculation occurs.

For further validation and exposing the weakness of the novel meanline modelling method, another experiment was performed by Harley et al[7]. Although the modelling process was for the same variety of turbocharger, automotive, the investigation was done on two new centrifugal compressors. For the purpose of this study, the meanline modelling was used.

On the one hand, the results obtained from the single-zone modelling process were predicted accurately for the larger compressor at low to medium tip speeds. However, there was a slightly difference in the prediction at the highest tip speeds. Moreover, the results obtained from the smaller compressor were not predicted accurately as the characteristic of the pressure ratio was insufficient towards surge. As far as the single passage computational fluid dynamics (CFD) method is concerned, the results have shown that the inlet circulation can be predicted with high accuracy; however, the method is incapable to predict the performance in the impeller trailing edge [7].

In a recent paper by Samkit et al[17], the preliminary design of a centrifugal compressor was investigated using non-dimensional method. The parameters' dimensions were calculated by various equations and correlations such as Weisner, Lame Ovals equations and Rodger and Sapiro[9], and Johnston and Dean [18] correlations. Moreover, a 3D centrifugal compressor was designed to validate the results of the theoretical analysis. The analysis and simulations indicated that there was a slight difference, about 9% in the results between CFD and the theoretical method. Although the obtained results were in a good agreement, the design losses were neglected from the theoretical calculations. Thus, the preliminary design procedure of the radial compressor is not accurate enough as the variation in the results would increase if the design losses were included.

Kerres et al [19] compared the performance of two types of 1D prediction models with numerical data for an automotive turbocharger centrifugal compressor with a vaneless diffuser and a scroll (Figure 1). The prediction models used for the comparison were suggested by Aungier [20] and Oh et al [21]. Moreover, the numerical results obtained by a 3D Reynolds-averaged Navier–Stokes (RANS) simulation for a small turbocharger compressor. The results of the comparison indicated that the 1D model were less accurate at low impeller speeds and choke than the computational fluid dynamics (CFD) 3D method; however, at high impeller speeds, they could predict precisely with a slight variation from the predictions of CFD calculations, see Figure 1.

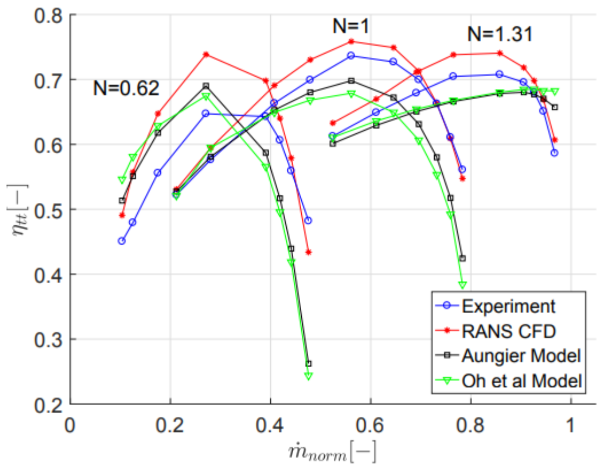

Figure 1: Isentropic Efficiency of Experiment compared with Reynolds-averaged Navier–Stokes (RANS) computational fluid dynamics (CFD), and the two prediction models.

Furthermore, Kerres et al [19] found that the loss model by Aungier could predict with higher accuracy than Oh et al [21]model. In addition, the results showed that the loss model collections could be improved, especially for jet-wake mixing and skin friction at high mass flows.

Moreover, an assessment of high-performance radial compressor parameters by 1D modelling and Reynolds-averaged Navier–Stokes (RANS) 3D computational fluid dynamics (CFD) simulation was done by Sundström et al [22]. A loss model and a steady state RANS model by Aungier [23] were chosen for the 1D modelling and computational fluid dynamics (CFD) calculations, respectively. Also, the centrifugal compressor examined was for automotive turbochargers, especially lightweight vehicles. The aim of the study was not only to quantify the variation between the predicted and the experimental data, but also to check the validation of the methodologies that were used.

Sundström et al [22] in Figure 2 found that the 1D method generated accurate results at design conditions; however, at higher speedlines towards surge and choke, there was a significant variation in the results. Figure 2 presents these variations at higher speedlines; N indicates the design speed of the compressor. Furthermore, the results for the validation of the used methodologies indicated that the impeller external loss was considerably higher in the computational fluid dynamics (CFD) calculations towards surge, but this loss could not be captured by 1D model, see Figure 3. Also, another significant difference was that the scroll loss was predicted larger in the 1D method. Finally, the authors suggested that by improving these major disparities in 1D modelling method, it would be beneficial as the accuracy of the prediction method could be improved.

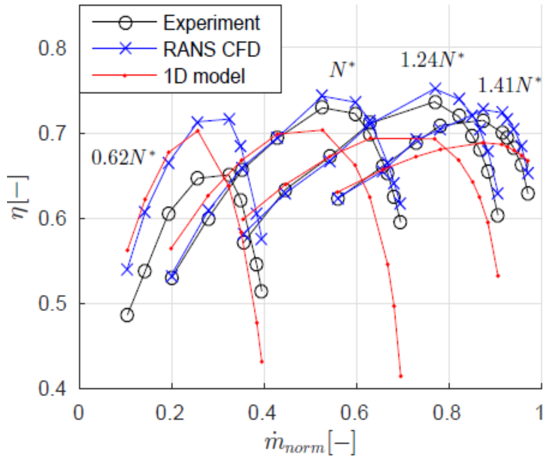

Figure 2. Comparison on the isentropic efficiency among experiment, Reynolds-averaged Navier–Stokes (RANS) computational fluid dynamics (CFD) and 1D model.

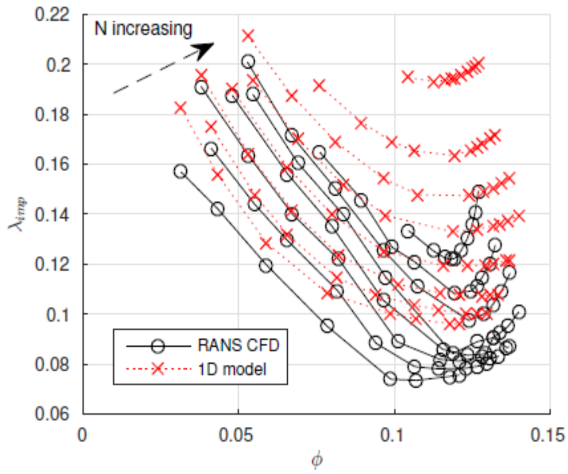

Figure 3: Impeller Losses of RANS CFD and 1D Model.

The present paper, therefore, is attempting to implement leading compressor preliminary performance zero-dimensional and pseudo one-dimensional techniques to the problem of implementation of these for turbocharger compressors which are electrically assisted.

2. Centrifugal compressor design methodology

The design target was an electric turbocharger compressor that could meet the boosting requirements of the engine at the specified engine speeds while offering a noticeable improvement in transient response. For the analysis of the turbocharger compressor flows, a one-dimensional approach was applied as it is not only a fast and reliable prediction model for centrifugal compressor, but also requires a small number of input parameters [19]. The 1D modelling method is based on the fundamental fluid flow equations, thermodynamic equations, and empirical correlations [23]. These equations were obtained from the Euler's turbomachinery theory and corresponding velocity diagrams, while the empirical relationships were obtained from experimental data. Also, in the 1D modelling approach, it was assumed that the flow conditions were uniform as the air would behave as an ideal gas [24].

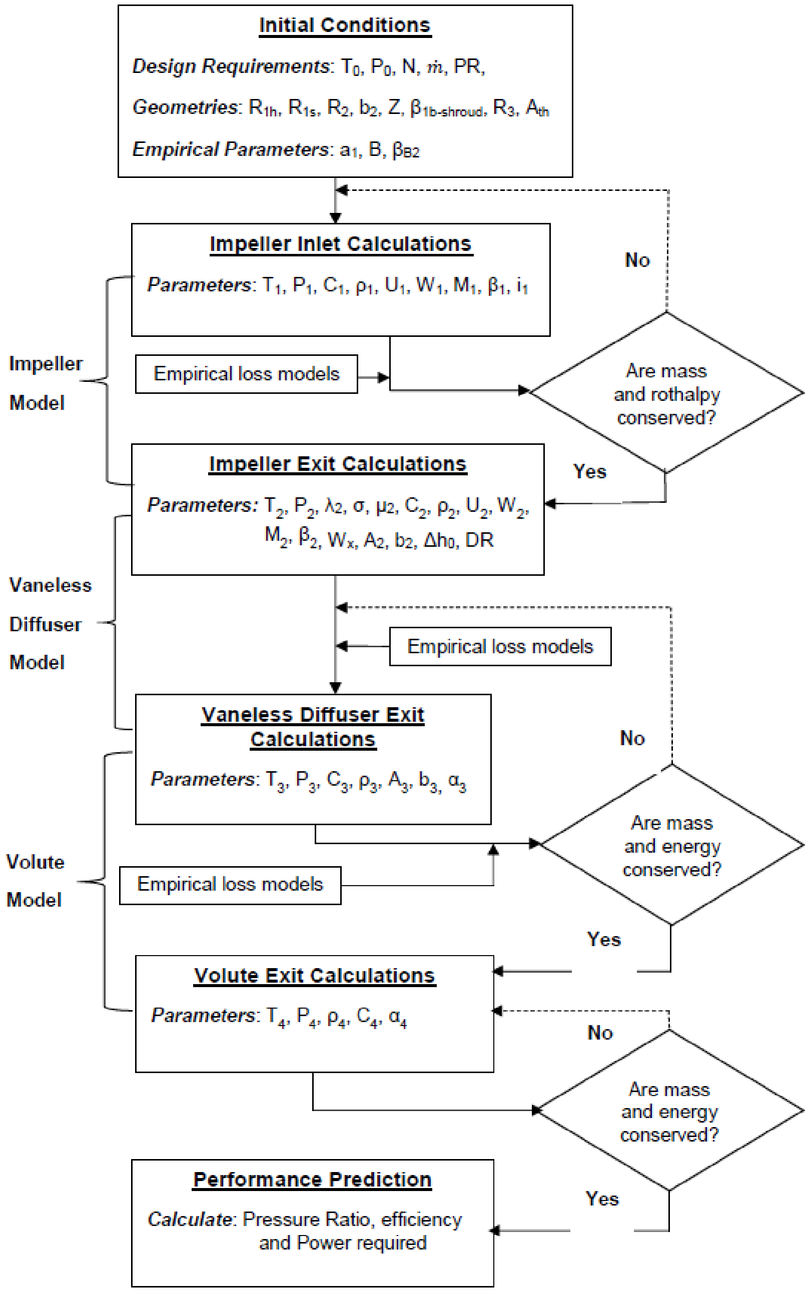

Figure 4: Compressor Modelling Procedure Flow Diagram.

In Figure 4, the schematic flow diagram of the compressor modelling procedure that was used for this analysis is shown, implemented in the MATLAB programming language. In addition, a crucial step for the modelling and analysis of the compressor was separating its individual components into four stages. Each stage includes the inlet or exit characteristics of the component. The compressor consists of the impeller, vaneless diffuser and the scroll. Thus, stage one is the impeller inlet, while stage two is the impeller exit and the vaneless diffuser inlet. The impeller exit and the vaneless diffuser operate under the same flow conditions. Moreover, stage three is the vaneless diffuser exit and the scroll inlet where the conditions are again the same. Finally, stage four is the scroll exit condition. In Figure 5, the cross-sectional schematic of the centrifugal compressor with the stage separation is shown.

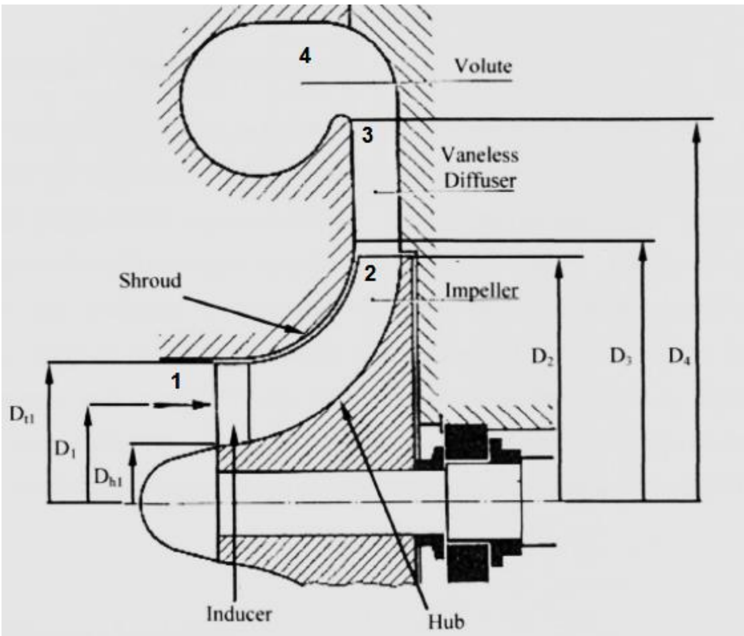

Figure 5. Centrifugal Compressor cross-section schematic labelling the stages.

To start the design procedure of the centrifugal compressor, the input parameters and the compressor geometry are required. Thus, the parameters that were given as designed constraints would be the inlet conditions (ambient static pressure and temperature), maximum rotational speed, air mass flow rate, and pressure ratio. As far as the compressor geometries were concerned they were obtained from the centrifugal compressor that was designed by Yang et al[4]. Both input parameters and compressor geometries are shown below.

Table 1. Operating conditions for the centrifugal compressor

Input Parameters	Metric Units
Ambient Static Pressure	1.01325 bar
Ambient Static Temperature	298 K
Maximum Rotational Speed	120000 rpm
Air Mass Flow Rate	0.08 kg/s
Pressure Ratio	2

Table 2. Main Compressor Geometry [4].

Geometrical Parameters	Values
Inlet hub radius R_{1h}	6.2 mm
Inlet shroud radius R_{1s}	17.2 mm
Impeller exit radius R_2	29.1 mm
Exit blade height b_2	3.4 mm

Blade number Z	5+5
Blade angle at inlet tip $\beta_{1b\text{-shroud}}$	-62 deg
Diffuser exit radius R_3	40.75 mm
Scroll throat A_{th}	397 ^{2}

3. Non-dimensional loss parameters

In this section, the non-dimensional loss models, $\overline{\omega}$, of the compressor components that were used for the purposes of the study were presented. Specifically, the loss models for each component were individually described and determined.

3.1 Impeller loss models

According to Aungier[23], the impeller losses can be converted and expressed as a total relative pressure loss defined as:

$$\Delta P_{tr} = f_c(P_{tr1} - P_{s1})\sum_i \overline{\omega}_i \tag{1}$$

Where f_c is a correction factor, which depends on the total relative density ρ_{tr}

The mathematical descriptions of these two functions according to Aungier[23] are described as:

$$f_c = \frac{\rho_{tr2}T_{tr2}}{\rho_{tr1}T_{tr1}} \tag{2}$$

$$\rho_{tr} = \frac{P_{tr}}{RT_{tr}} \tag{3}$$

As the impeller is the rotating component, it was essential to determine the total relative pressure and temperature, which are defined as follows [19]:

$$P_{tr} = P_s\left[1 + \left(\frac{\gamma - 1}{2}\right)M_r^2\right]^{\frac{\gamma}{\gamma-1}} \tag{4}$$

$$T_{tr} = T_s\left[1 + \left(\frac{\gamma - 1}{2}\right)M_r^2\right] \tag{5}$$

Where M_r is the relative Mach number, defined as:

$$M_r = \frac{W}{\sqrt{\gamma R T_s}} \tag{6}$$

To calculate the actual conditions of the impeller, the non-dimensional losses need to be subtracted from the isentropic conditions. However, the total relative temperatures in isentropic and actual flow are the same because the rothalpy is conserved. Thus, as far as the total relative pressure in the actual flow at the second stage is concerned, it can be calculated by subtracting the total relative pressure losses from the total relative pressure in the isentropic process. The equation is shown below[23]:

$$P_{tr2} = P_{tr2,is} - \Delta P_{tr} \tag{7}$$

Furthermore, according to Bathie[25], the total pressure and temperature at the throat are described as:

$$T_{th} = T_{t1} - \left[\frac{2N\pi(C_{u1}r_{m1} - C_{uth}r_{mth})}{60c_p}\right] \tag{8}$$

$$P_{th} = P_{t1}\left(\frac{T_{th}}{T_{t1}}\right)^{\frac{\gamma}{\gamma-1}} \tag{9}$$

Aungier[23] and Boyce [26] loss models were selected to determine the loss parameters of the impeller. The chosen models that are analysed are presented in Table 1.

Table 1. Impeller Loss Models used for the study[23][26].

Impeller Loss Models	
1. Shock	2. Incidence
3. Diffusion	4. Choke
5. Skin friction	6. Clearance gap
7. Blade loading	8. Hub-shroud loading
9. Wake mixing	10. Expansion
11. Supercritical Mach number	

Moreover, each loss parameter was described and analysed individually. Also, the loss model was described as a function of inlet, throat, isentropic exit and boundary conditions such as the area, the radius of the impeller, the rotational speed and the mass flow rate.

3.2 Vaneless diffuser loss models

According to Aungier[23], the non-dimensional vaneless diffuser losses can be converted and expressed as a total pressure loss defined as:

$$\Delta P_{t3} = (P_{t2} - P_{s2})\sum_i \bar{\omega}_i \tag{10}$$

The vaneless diffuser loss model process is similar to that in the impeller. However, the vaneless diffuser is a stationary component and the rothalpy is decreased to a constant enthalpy, hence the total temperature in the vaneless diffuser and the scroll is constant.

The actual conditions of the vaneless diffuser were calculated by subtracting the total pressure loss from the isentropic total pressure. The equation is shown below[23]:

$$P_{t3} = P_{t3,is} - \Delta P_{t3} \tag{11}$$

Furthermore, two loss parameters were selected to model the losses for the vaneless diffuser, the skin friction and diffusion[23].

Table 2. Vaneless diffuser loss models

Vaneless Diffuser Loss Models	
1. Skin friction	2. Diffusion

3.3 Scroll loss models

According to Aungier[23], the non-dimensional scroll losses can be converted and expressed as a total pressure loss defined as:

$$\Delta P_{t4} = (P_{t3} - P_{s3}) \sum_i \bar{\omega}_i \tag{12}$$

As stated in the previous vaneless diffuser section, the scroll is in stationary form, hence the total temperature in the scroll is constant. Furthermore, to calculate the actual pressure conditions of the scroll, the non-dimensional pressure losses need to be subtracted from the isentropic conditions. The equation is shown below[23]:

$$P_{t4} = P_{t4,is} - \Delta P_{t4} \tag{13}$$

Moreover, it has been stated that there are four non-dimensional scroll losses[23].

Table 3. Scroll loss models

Scroll Loss Models	
1. Meridional velocity loss	2. Tangential velocity loss
3. Skin friction	4. Exit cone loss

4. Modeling the engine

For the aim of this study, two models of an engine were designed in GT-Power. The first model was sourced from an available model of the Ford Ecoboost 1.5L, an inline 3-cylinder engine which served as the baseline model with the correct turbocharger map implemented in the model. The second model had the same engine but with the EAT implemented. The second model is shown in Figure .

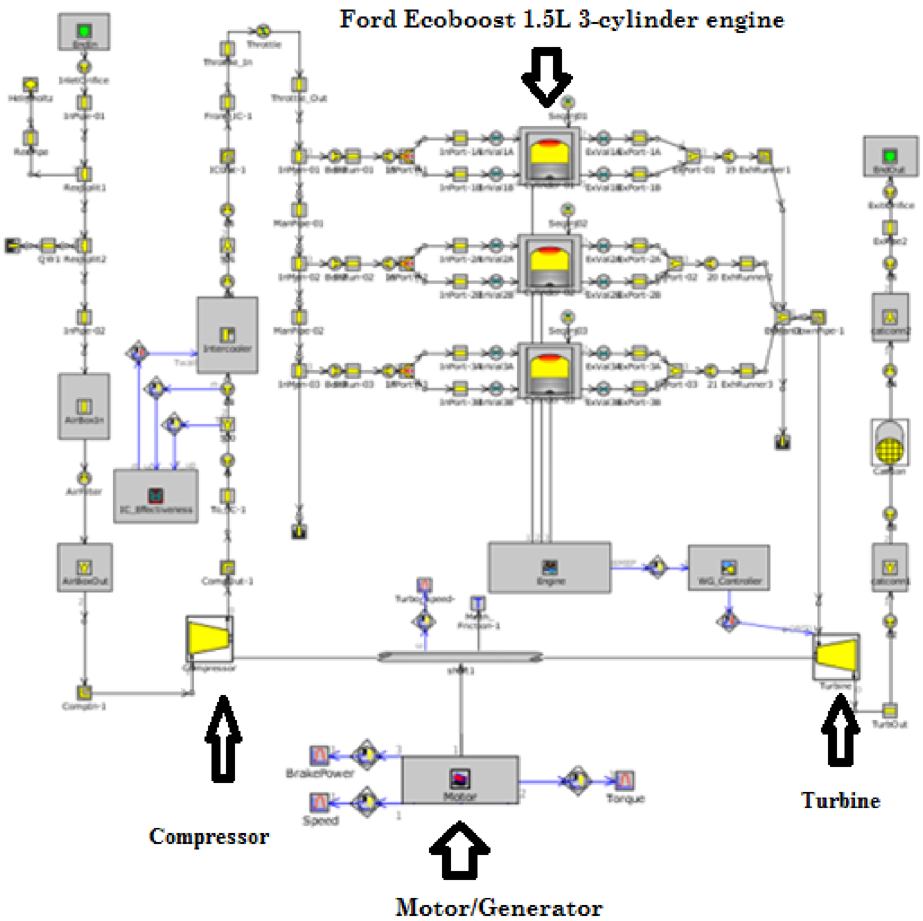

Figure 6: Model of the Ford Ecoboost 1.5L electrically assisted turbocharged engine.

In the above model the motor/generator object, which represents the electrical machine of the electrically assisted turbocharger, is attached to the turboshaft.

4.1Motor/Generator specifications

The motor/generator parameters used for the simulation were based on an electrical machine developed by Lee and Ehsani[27]. Table 4 below shows the Brushless DC motor/generator specifications while Figure 7 illustrates the peak power and torque curves of the engine modelled.

Table 4: Motor/Generator Specifications.

Attribute	Object value	Units
Torque Constant	0.0042	N.m/A
Equivalent Resistance	3	Ohm
Equivalent Inductance	1.22	mH
Friction Torque	0.662	N.m
Stall Current	200	A
Inertia	8.2614e – 5	kgm²

Furthermore, the applied voltage of the battery that was used to the engine model was 48V. The development of electric turbocharger was initially based (and limited by) the 12V architecture of automobiles. However, some automobile makers have been considering the use of 48V architectures to enhance the goal of improving transient response for a considerable time in order to accommodate mild-hybridization requirements. According to a simulation that was conducted by Nishiwaki et al [28] for a 48V battery system and compared against an equivalent 12V architecture, have shown a significant improvement in the transient response at low engine speeds (0.4s to reach a target 1.65 pressure ratio against 1.0s for the 12V system).

Finally, for the analysis presented here, it is worth noting that the thermal behavior of the motor/generator was ignored.

4.2 Engine Specifications

For the simulation of the modeled engine, it was required to import the Ford Ecoboost 1.5L specifications for modeling the engine objects. The specifications are described below.

Table 5. Ford Focus, Ecoboost 1.5L, 3-cylinder petrol engine specification [29]

Attribute	Object value	Unit
Bore	83	Mm
Stroke	92.4	Mm
Connecting Rod Length	137	Mm
Compression Ratio	10.4	----
TDC Clearance Height	1	mm
Max.Brake Power	110	kW
Max. Brake Torque	240	Nm
Min. Brake Specific Fuel Consumption (@3000rpm)	234	g/kWh
Valves	4	

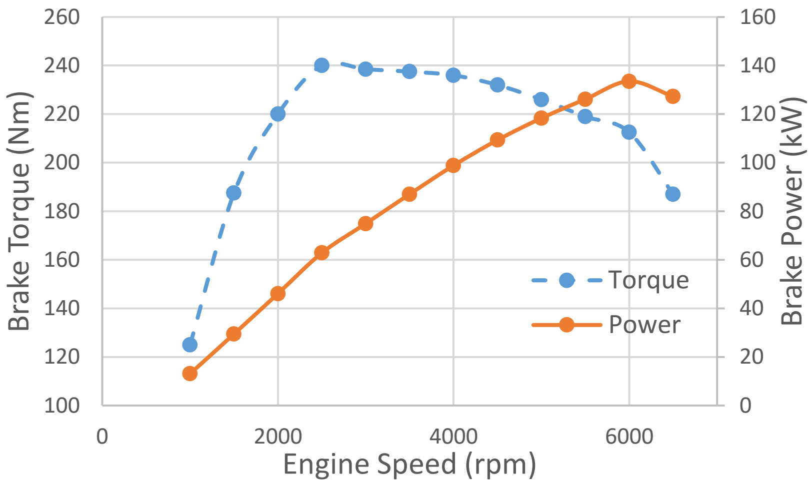

Figure 7: Performance of the based turbo-charged engine.

4.3 Description of the simulation

Five cases were used for the simulation of the baseline model and electrically assisted turbocharged model. Each case had different engine speed which was varied from 1000 to 5000 rpm. Moreover, as initial conditions were given, the ambient pressure and temperature were1.01325 bar and 298K, respectively.

It is worth to be mentioned that the model of the electrically assisted turbocharger was modified and analysed for five different power levels, varied from 1kW to 5kW. This is performed to study and examine how the power consumed or generated from or by the electrical machine affects the engine torque at low and high engine speed rates. The operating point used for the simulations are presented in Table 6.

Table 6. The operating points that were used for the simulation

Operating Point	Turbocharger	Maximum Power
Baseline	Conventional	-
Operating Point 1	EAT	1kW
Operating Point 2	EAT	2 kW
Operating Point 3	EAT	3 kW
Operating Point 4	EAT	4 kW
Operating Point 5	EAT	5 kW

5. Results and Discussion

5.1 Compressor Efficiency

The operation of the centrifugal compressor for the baseline and EAT models at low engine speed rates, 1000 rpm and 2000 rpm, are presented in the following figures – the outcome of the engine simulation setup described in Section 5.

Figure shows that the operation of the compressor at 1000 rpm engine speed is moved significantly to the right side of the performance map with the assistance of the motor/generator. Thus, the compressor operation has moved to a more efficient region. Moderate improvement can be observed to the operation for the 1kW and 2kW EAT model compared to the baseline model. On the other hand, from 3kW to 5kW power models, the compressor operation has increased greatly compared to the baseline model.

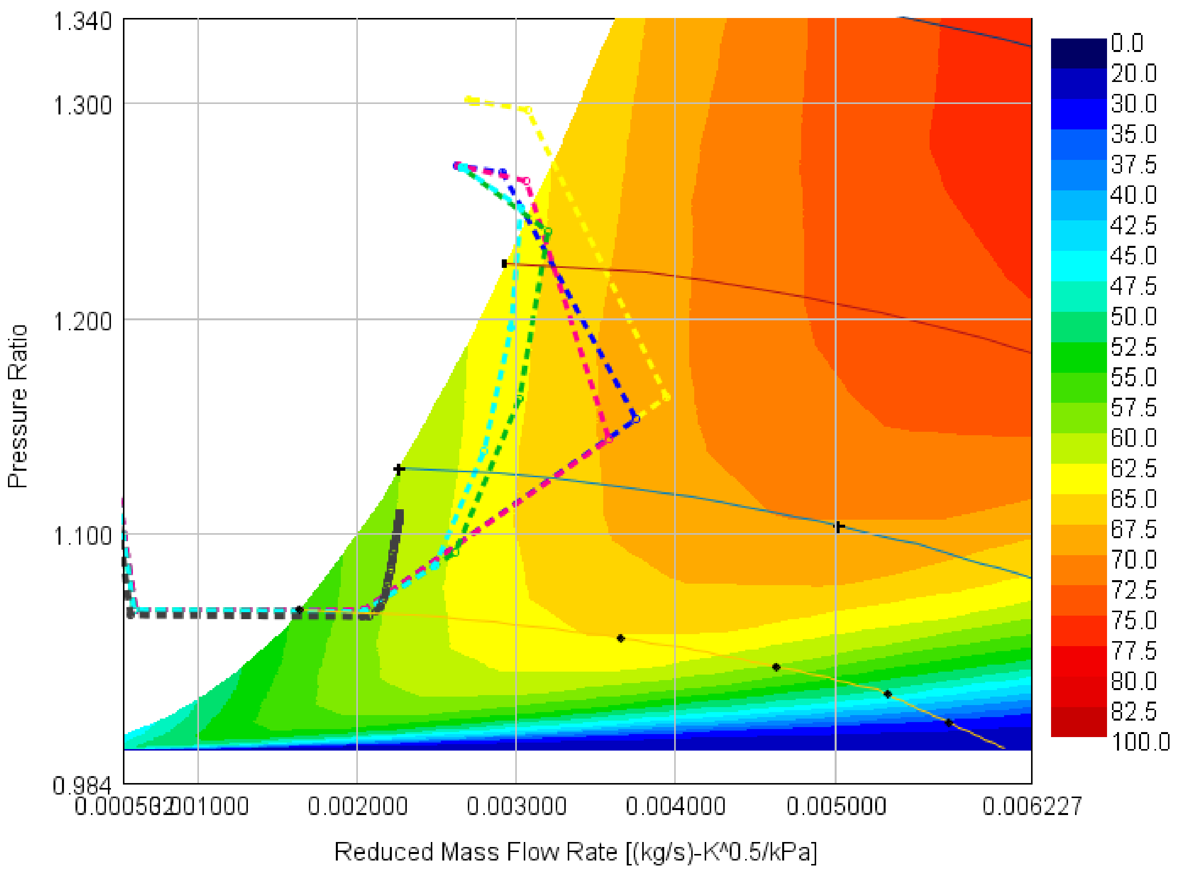

Figure 8: Compressor Performance at 1000 rpm engine speed with efficiency contours.

Furthermore, an important drawback is that the EAT forces the operation of the compressor to exceed the surge line of the efficiency map as is shown in Figure . Therefore, map enhancement techniques should be applied to the compressor, such as casing treatment, to overcome this drawback.

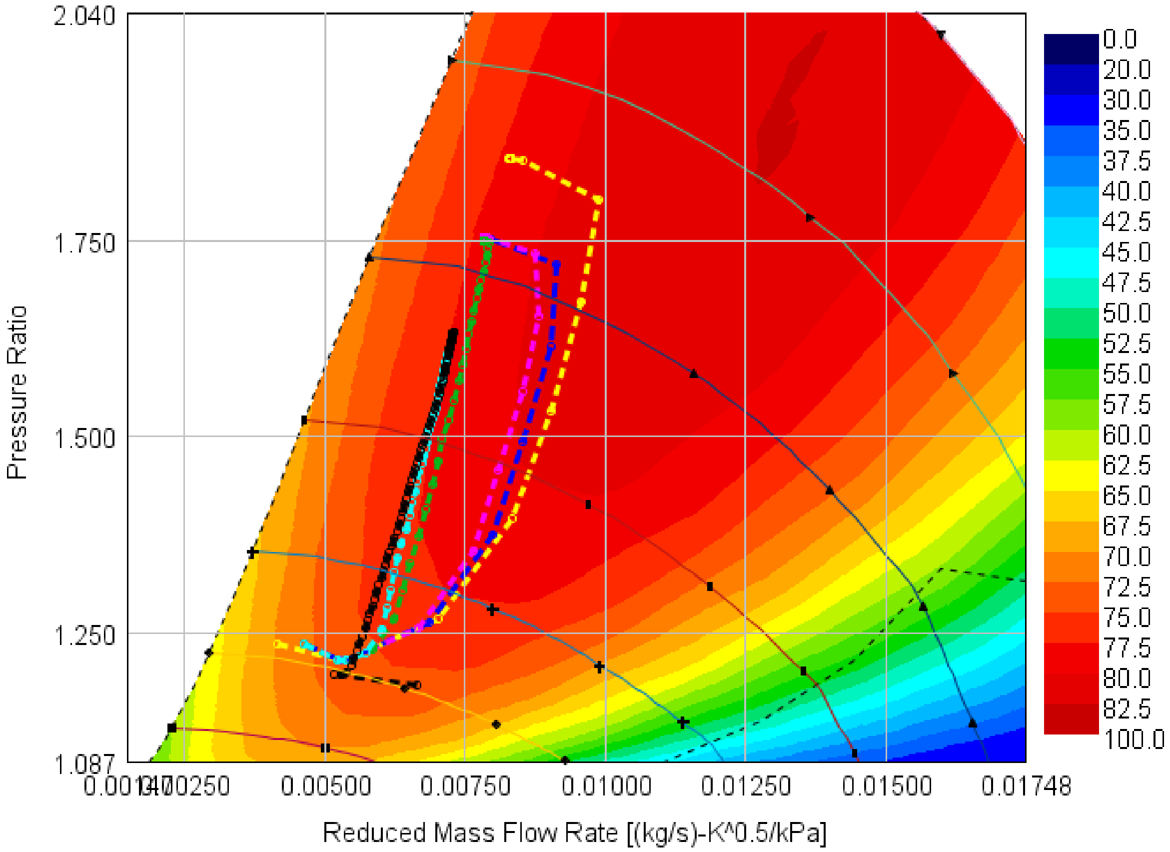

Figure 9: Compressor Performance at 2000 rpm engine speed.

As far as the 2000 rpm engine speed is concerned, Figure illustrates that the application of the motor/generator to the turbocharger shaft pushes the operation of the centrifugal compressor towards the right side of the map. Thus, the compressor operates to a more efficient area. Also, Figure shows that the electrically-assisted turbocharger (EAT) models, except from the 1kW model, have significantly increased the pressure ratio of the compressor, resulting in further improvement of the engine performance.

5.2 Transient Response

As can be seen from Figure 13, the transient response time of the baseline engine at 1000 rpm has been reduced by 85.6% with the electrical assistance of 5kW (for accelerations to 110,000 rpm out of a maximum turbocharger speed of 120,000 rpm). Moreover, the 3kW and the 4kW models have almost the same transient response time as the 5kW. On the other hand, the transient response time for 2kW configuration has been decreased by 64% compared to baseline model. It is worth to be mentioned that the application of the electrical assisted turbocharger with 1kW reduced only 20% of the response time for the engine compared to the conventional turbocharger. Therefore, it is essential to install at least a 2kW EAT to improve the performance of the engine considerably.

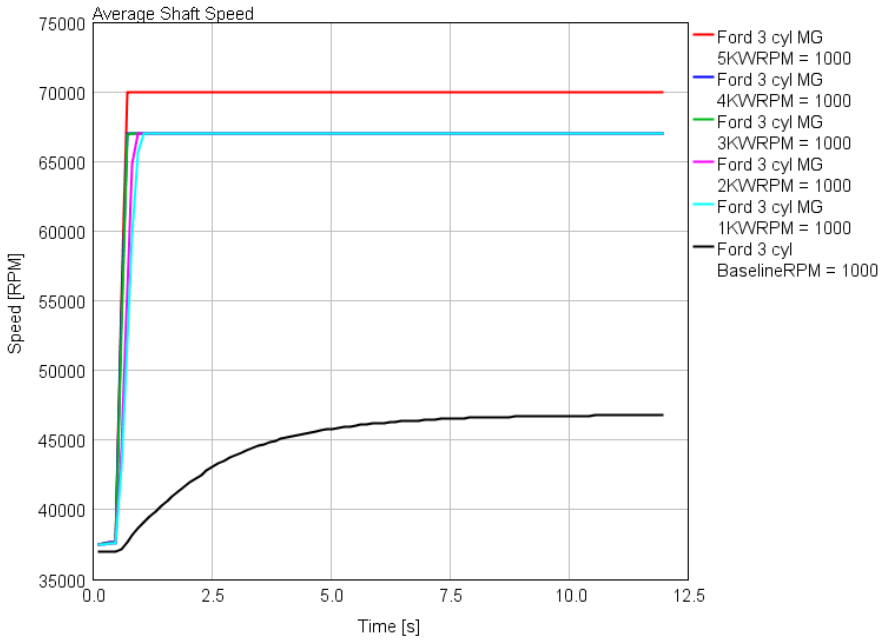

Figure 10: Turbocharger shaft speed at 1000 rpm engine.

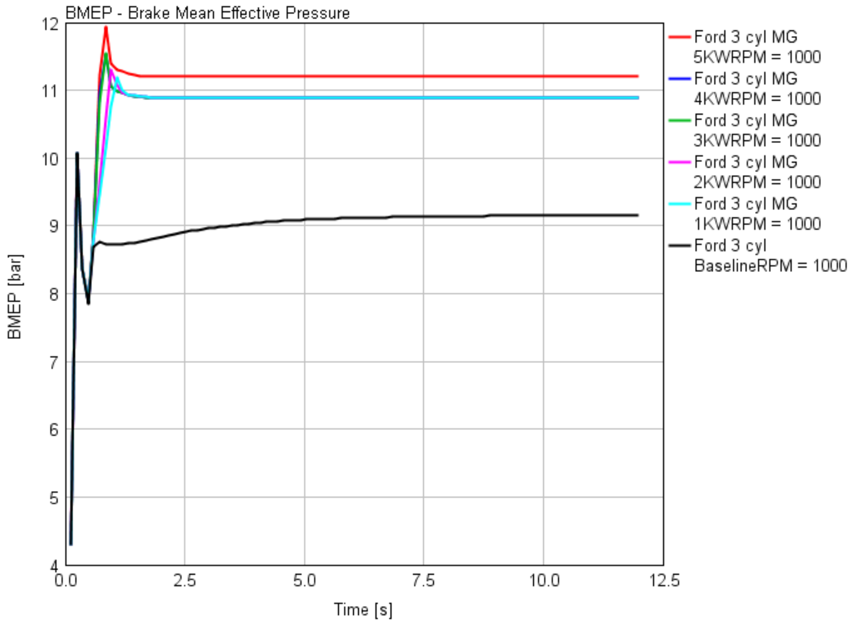

Figure 11: Brake Mean Effective Pressure (BMEP) response time at 1000 rpm engine speed.

The results in Figure 10 indicate that the electrical assisted turbocharger of 1kW at 1000 rpm of engine speed, can decrease the transient response time of the engine by 78.4% whereas with higher power modifications the response time can be reduced up to 83.2%. Moreover, the fluctuations that are displayed on the graphs in Figure 11 were a result of the mass flow rate variation due to the throttle valve opening. In addition, as can be seen from Figure 11, there is an insignificant effect on the reduction of the response time among the 3kW and the higher power level models.

Furthermore, the results from Figure 12 indicate that as the power levels rise, not only is the response time of the engine decreased, but the BMEP is also increased significantly.

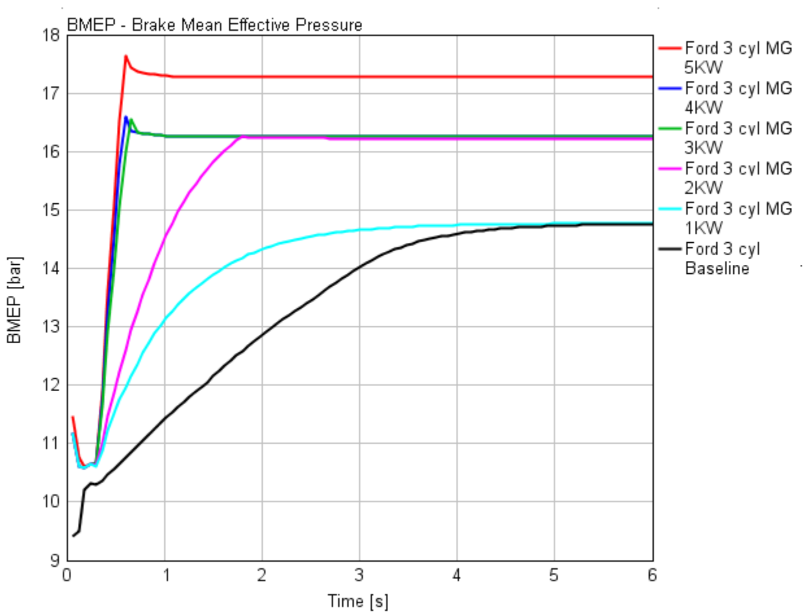

Figure 12: Brake Mean Effective Pressure response time at 2000 rpm engine speed.

In Figure , the average turbocharger shaft speed over time is illustrated. Overall, the shaft speed is rapidly increased with the electrical assistance. Especially, the maximum shaft speed that was achieved by the 5kW model peaked at 110 krpm, while the maximum speed for the models from 2kW to 4kW was at 105 krpm. Although the shaft speed of 1kW configuration has been increased faster than the conventional turbocharger, the maximum speed that was achieved was lower than that of the baseline model. Thus, the 1kW model is not a preferable turbocharger for the engine.

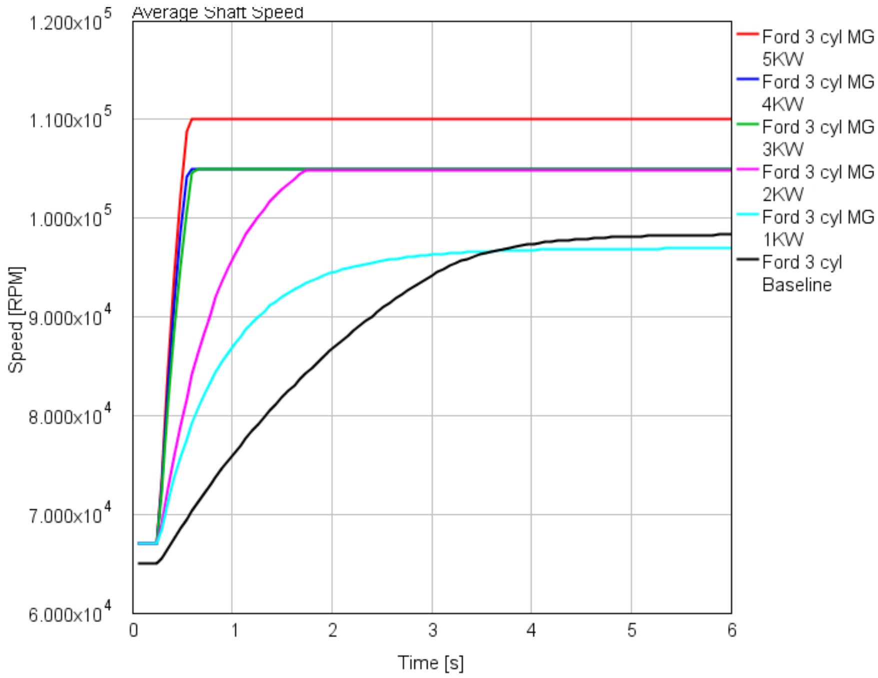

Figure 13: Turbocharger shaft speed at 2000 rpm engine speed.

5.3 Brake Torque and BSFC graphs

In this section, the brake torque and the brake specific fuel consumption of the GT-Power models over the engine speed graphs are presented and discussed. The results in Figure 14 indicate that engine torque was significantly improved with the electrically assisted turbocharger. Especially, the highest value of torque achieved by the 5kW model was at 240 Nm at 3000 rpm engine speed. Moreover, the torque graphs of the 3kW and 4kW model were almost the same, but, nonetheless, the difference can be spotted in the netBSFC map in Figure (after power required to run the motor was subtracted). The BSFC of the 4kW power level is slightly reduced for the engine speed range from 3000 to 4000 rpm compared to the 3kW EAT model.

Furthermore, as far as the 1kW and 2kW cases are concerned, the engine torque has been increased for both models, however, only for the engine range of 1000-2000 rpm and 1000-3000 rpm, respectively. It is worth noting that at 4000 to 5000 rpm, the torque of the EAT models has been decreased and have slight differences with the engine torque of the baseline model as can been seen in Figure 14. This occurs because the electrical assisted turbocharger extracts torque from the shaft at high engine speed to charge the battery of the electric machine.

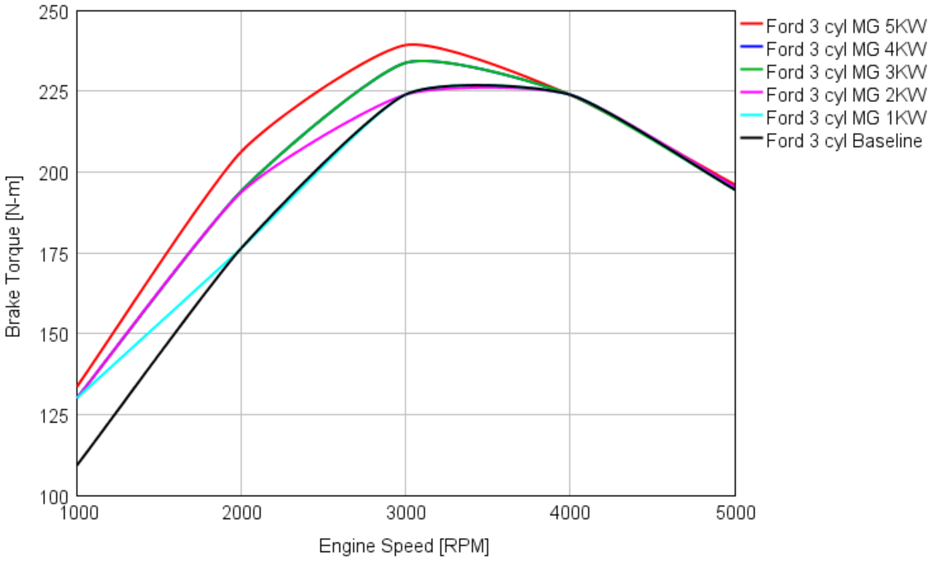

Figure 14. Engine Torque results from the engine model.

The results in Figure depict the BSFC of GT-Power models. It is evident that when the EAT is applied, the BSFC of the engine is significantly improved. Specifically, for the 5kW model, the BSFC has been reduced by an average of 1.4% compared to the baseline model. In addition, the 1kW has considerably decreased the BSFC for 1000-4000 rpm speed range whereas the BSFC has been further reduced with the electrical assistance of 2kW. Finally, at high engine speed, there is a slight fall in the BSFC graphs of the electrically-assisted turbocharger (EAT) models and the baseline model despite the fact that additional torque is extracted from the engine.

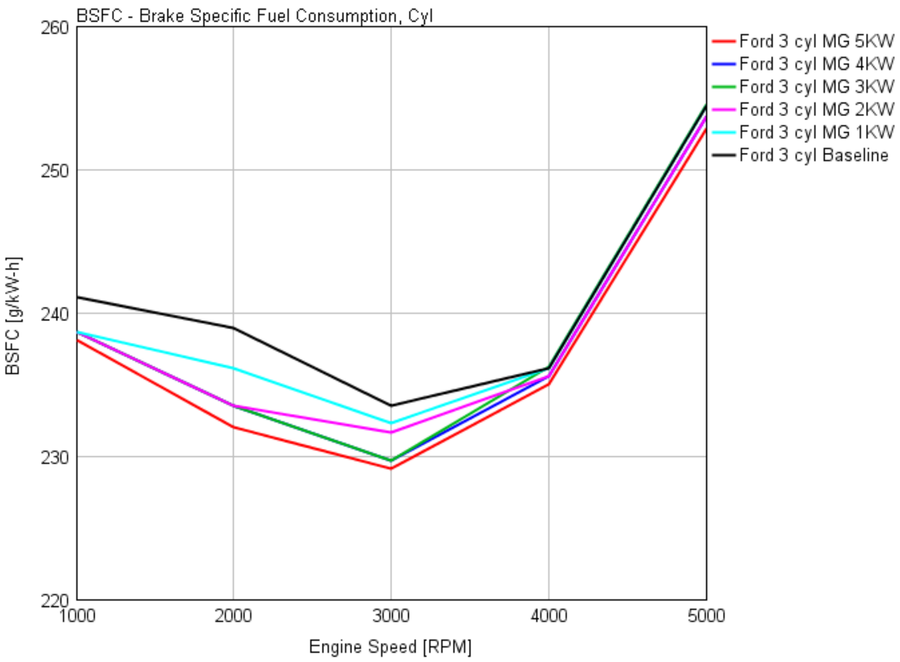

Figure 15: BSFC map results from the engine model.

6. Results from the optimised compressor

In this section, the results obtained from GT-Power simulation for the optimised compressor which was found by using the Matlab code are presented and discussed. Table 8 includes the optimised geometries of the centrifugal compressor which were obtained from the Matlab code.

Table 8: Optimisation results for B=0.02 and N=120,000 rpm.

$r_{1h}[m]$	0.001	$Z_r[-]$	10
$r_{1t}[m]$	0.0113	$\beta_{B2}[^o]$	-45
$M_{1t}[-]$	0.7015	$DR[-]$	1.6682
$\beta_1[^o]$	15.1548	$n_{stage}[-]$	0.4361
$A_{f1}[m^2]$	3.9555e-4	$b_2[m]$	0.0047
$U_{1t}[m/s]$	141.5642	$r_2[m]$	0.0294
$W_{1t}[m/s]$	231.0347	$U_2[m/s]$	369.6808
$C_{m1}[m/s]$	223	$W_2[m/s]$	138.4913
$C_{u1}[m/s]$	81.1653	$M_2[-]$	0.6807
$C_1[m/s]$	237.3116		

These geometries were applied to the GT-Power models to evaluate the effect of the optimised compressor to the engine performance. In addition, to identify the differences between the initial and the optimised compressor a one by one comparison of the models was conducted.

6.1 Comparison of the baseline models

The results in Figure 16 shows that overall, there was a slight increase in the engine torque with the optimised compressor. However, at high engine speed and especially from 4000 to 5000 rpm the engine torque has been moderately risen. Similarly, in Figure 17 the BSFC for the optimised compressor has been slightly improved compared with the BSFC of the initial compressor.

Moreover, there was not any reduction to the transient response time of the engine with the optimised compressor. However, the turbocharger shaft speed for 1000rpm engine speed has been peaked to a higher value than the initial compressor design as is shown in Figure 18.

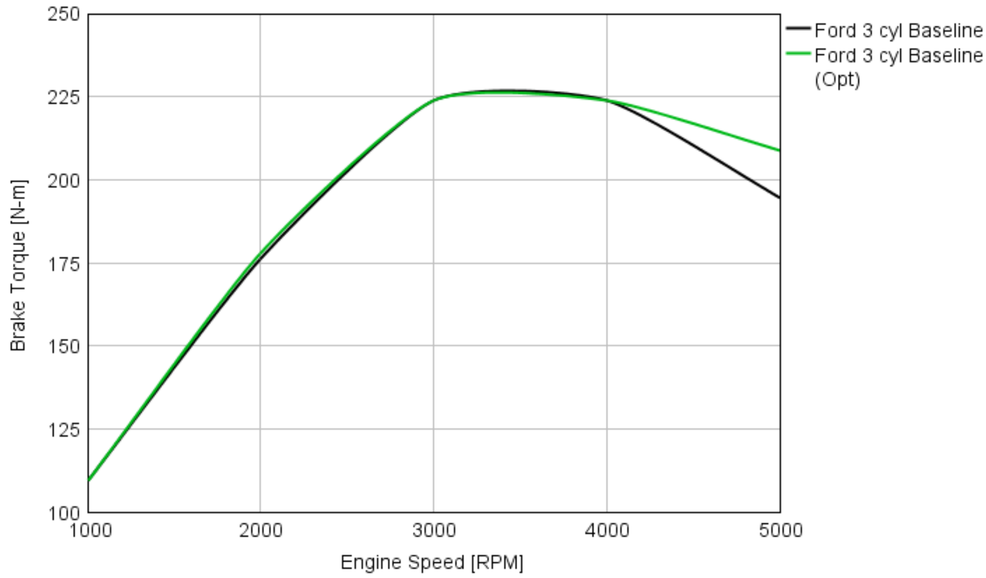

Figure 16: Brake torque versus engine speed for the initial and the optimised baseline models.

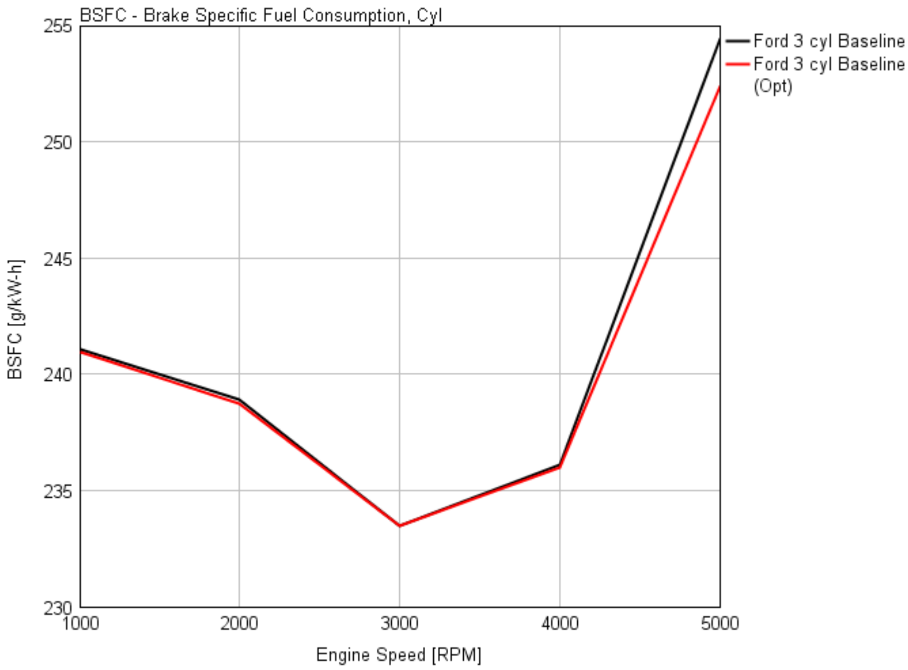

Figure 17: BSFC graphs for the initial and optimised baseline models.

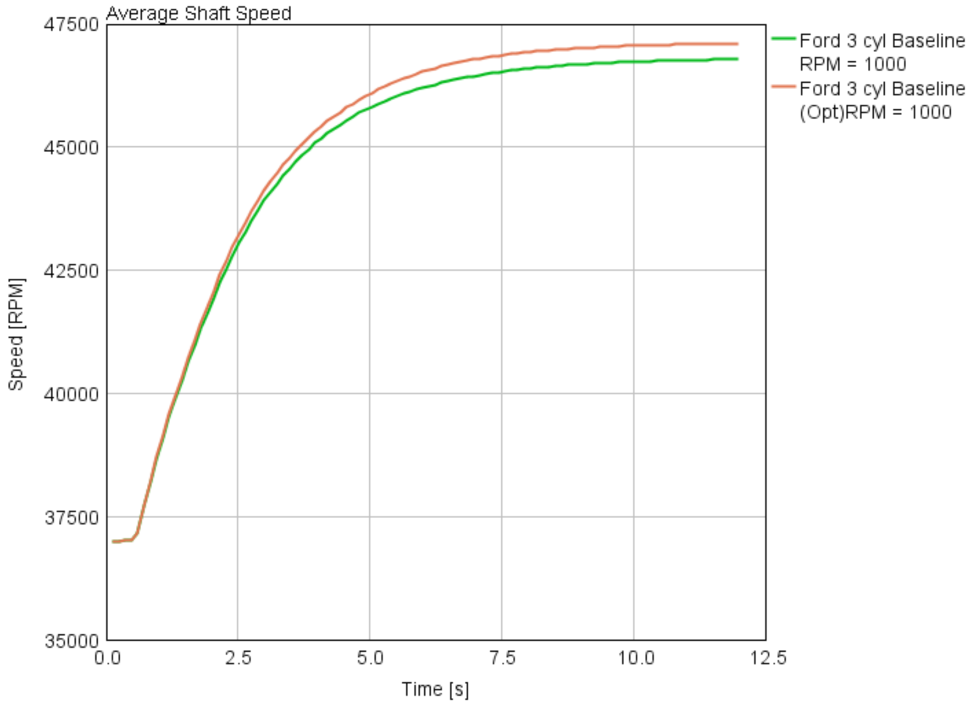

Figure 18: Average Shaft speed of the baseline models at 1000 rpm engine speed.

6.2 Comparison of the EAT with 1kW power level models

The results obtained from the simulations for the initial and optimised compressor of the electrical assisted turbocharger models with power level 1kW indicate that there is no significant difference between the two compressors. Figure 19 shows the engine torque versus engine speed for both centrifugal compressors. Even though the two graphs are very similar, there is a slight rise of the torque for the optimised compressor at engine speed range of 4000-5000rpm.

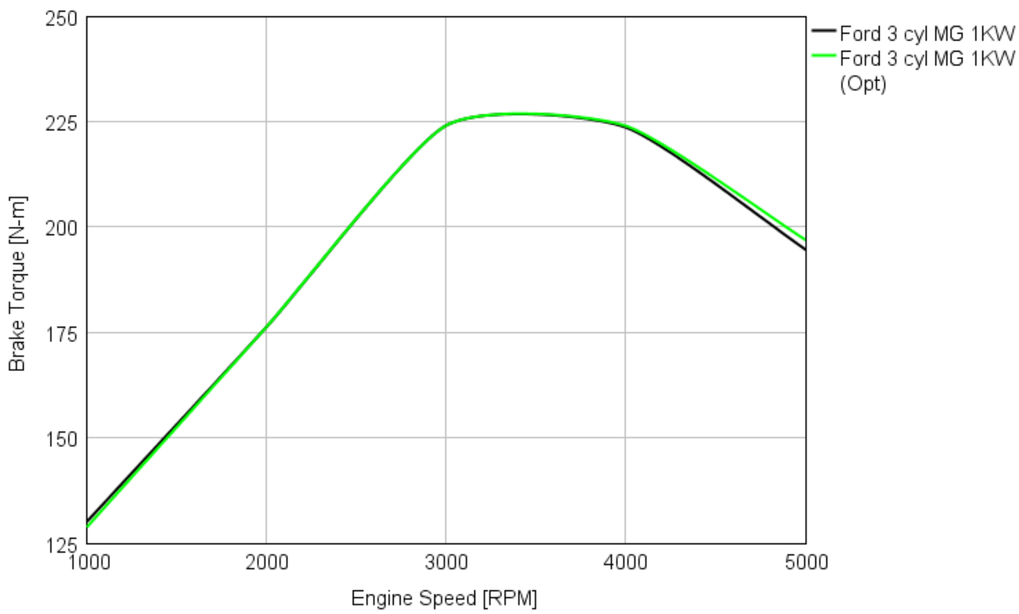

Figure 19: Brake torque over engine speed for the initial and the optimised EAT 1kW models.

Similarly, as can been seen from Figure 20 the BSFC for both compressors are almost the same except for the engine speed range of 1000-2000 rpm in which the BSFC of the optimised compressor has been slightly increased. However, the results indicated that with the optimised compressor there is an insignificant improvement in the engine performance.

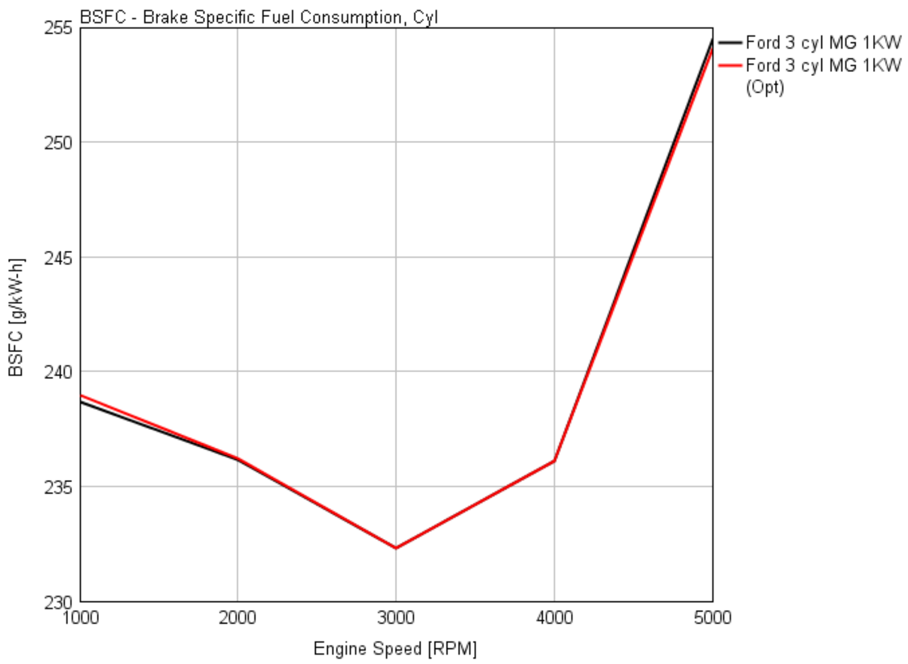

Figure 20: BSFC graphs for the initial and optimised EAT 1kW models.

6.3 Comparison of the EAT with 2kW power level models

The optimised compressor in the EAT model with 2kW power level configuration has significantly improved the overall performance of the engine. Especially, as shown in Figure 21, from 2000 to 4000 rpm the engine torque of the optimised compressor has increased moderately compared to the initial design of the compressor. On the other hand, at low engine speed the brake torque for both compressors was the same while at high engine speed the initial compressor had greater engine torque than the optimised compressor.

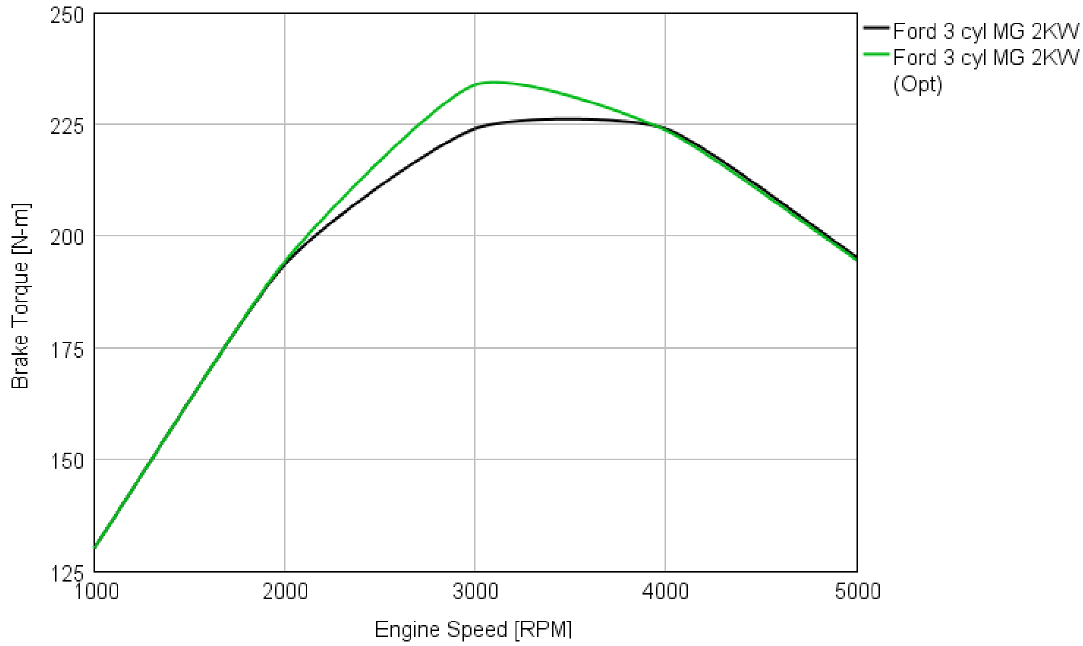

Figure 21: Brake Torque graphs for the initial (black) and optimised (green) EAT 2kW models.

The graphs in Figure 22 present the BSFC over the engine speed for the initial and the optimised compressor. It is evident that at the engine speed range of 2000 rpm-4000 rpm the brake specific fuel consumption (BSFC) has been considerably reduced with the optimised compressor while at high engine speed the brake specific fuel consumption (BSFC) is slightly increased compared to the initial compressor. Moreover, the results in Figure 23 indicate that the transient response time of the engine model with the optimised compressor has been reduced by 25%.

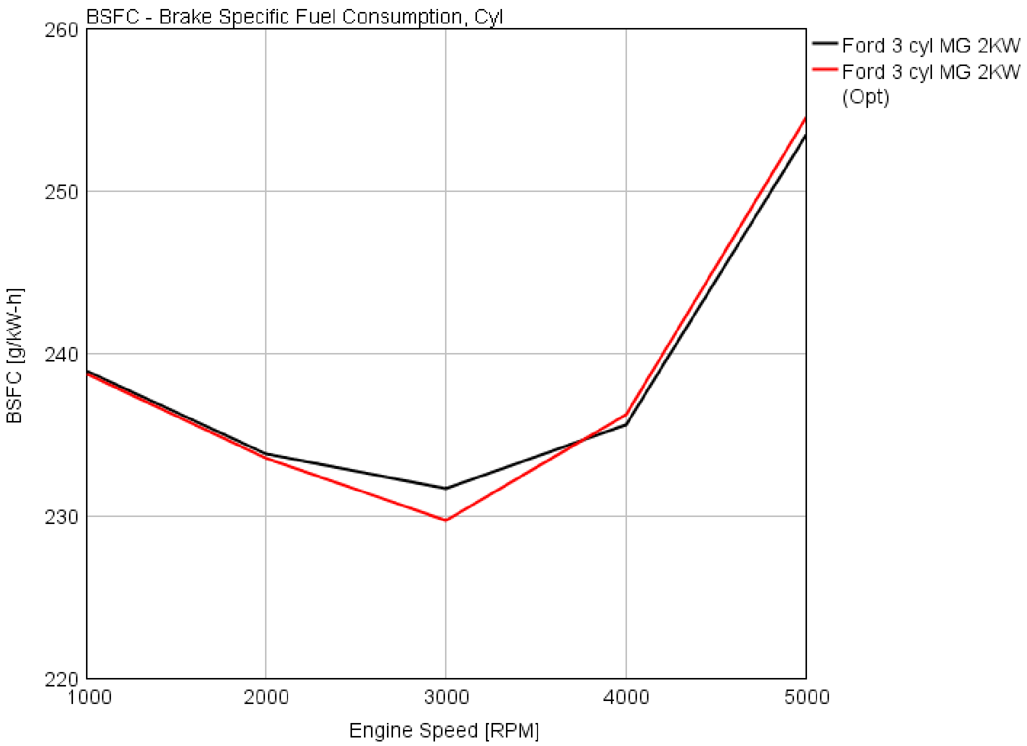

462
463 **Figure 22**: BSFC graphs for the initial and optimised EAT 2kW models.

464

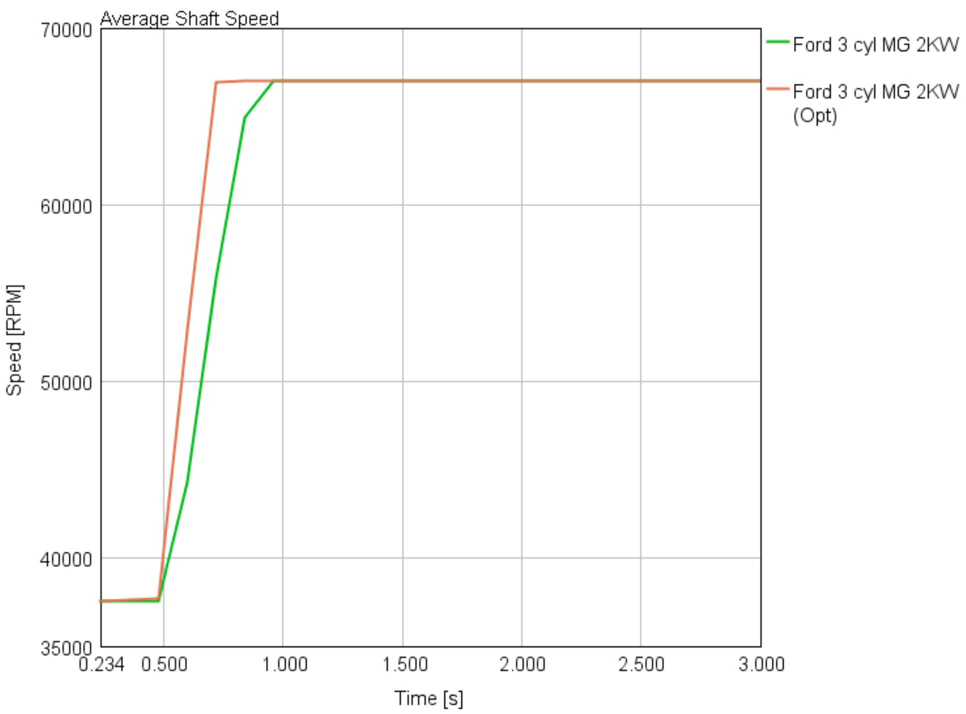

465
466 **Figure 23**: Average Shaft speed of the electrically-assisted turbocharger (EAT) models with
467 2kW power level at 1000 rpm engine speed.

468

6.4 Comparison of the EAT with 3kW and 4kW power level models

The results obtained from the GT-Power simulations show that in the electrically-assisted turbocharger (EAT) models of 3kW despite the change on the compressor, the engine performance remained steady. Similarly, it has been found that the electrically-assisted turbocharger (EAT) model of 4kW with the optimised compressor has the same results with the initial compressor model. In the following figures, some results of the 3kW as well the 4kW models are presented.

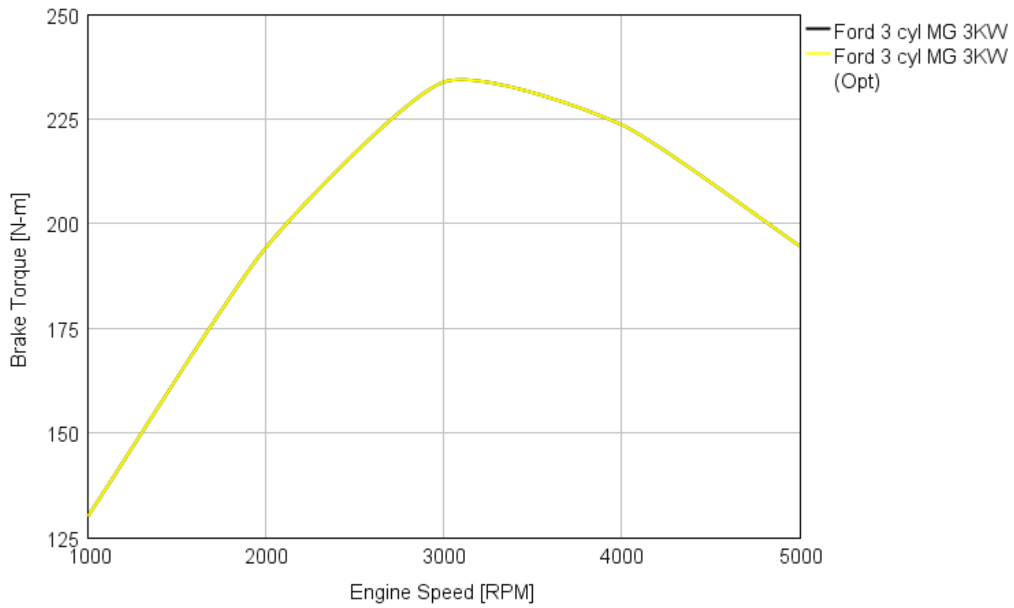

Figure 24: Brake Torque of the electrically-assisted turbocharger (EAT) 3kW model for the initial and optimised compressor.

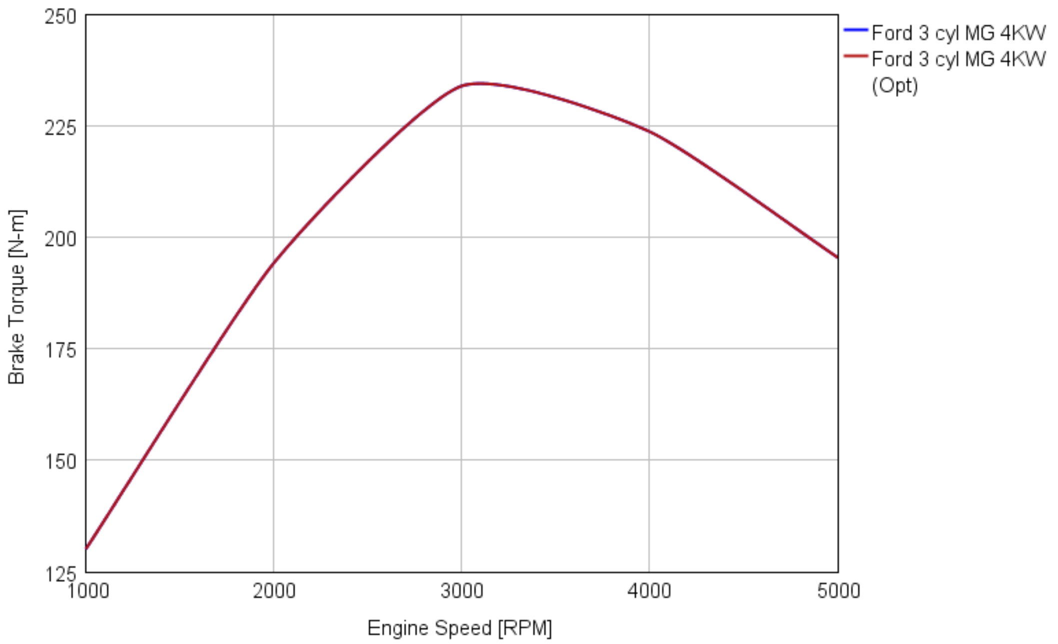

Figure 25: Brake Torque of the electrically-assisted turbocharger (EAT) 4kW model for the initial and optimised compressor.

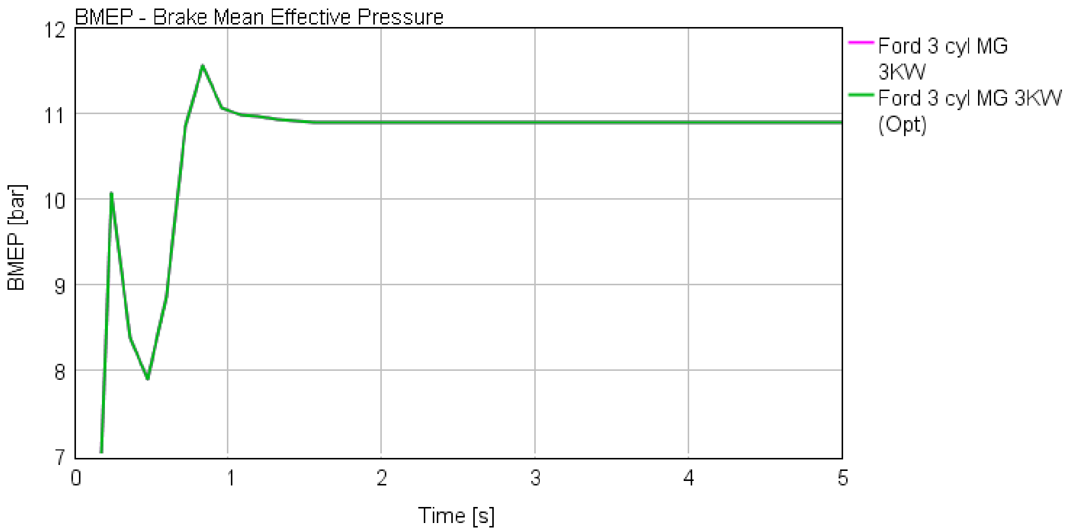

Figure 26: Brake mean effective pump (BMEP) graphs of the EAT 3kW model for the initial and optimised compressor.

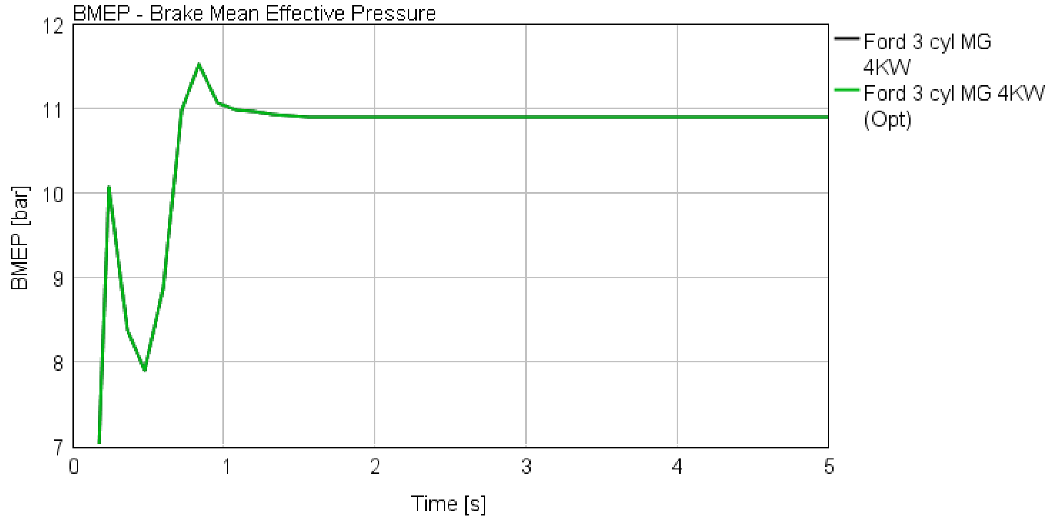

Figure 27: Brake mean effective pressure (BMEP) graphs of the EAT 4kW model for the initial and optimised compressor.

As can be seen from the above figures, the results of the baseline and optimised compressor totally match for both modelling cases 3kW and 4kW. One plausible reason for the results that occurred could be an error in the simulations for these cases. Moreover, another explanation could be that in the optimised compressor the exit diameter of the impeller was slightly reduced, hence the change did not affect significantly the performance of the engine, as in the electrically-assisted turbocharger (EAT) 1kW case.

6.5 Comparison of the EAT with 5kW power level models

In this section, a comparison between the engine model with the optimised compressor and the engine model with the initial compressor was conducted. Figure 28, presents the brake torque of the two models versus engine speed. It is clear that the engine torque has considerably risen with optimised centrifugal compressor in place. Especially from 1000 rpm the engine torque is increased gradually until 3000 rpm where the engine torque is peaked at 293.2N. However, from 4000 to 5000 rpm the torque is decreased sharply and matches with the values of the torque of the engine model with initial compressor.

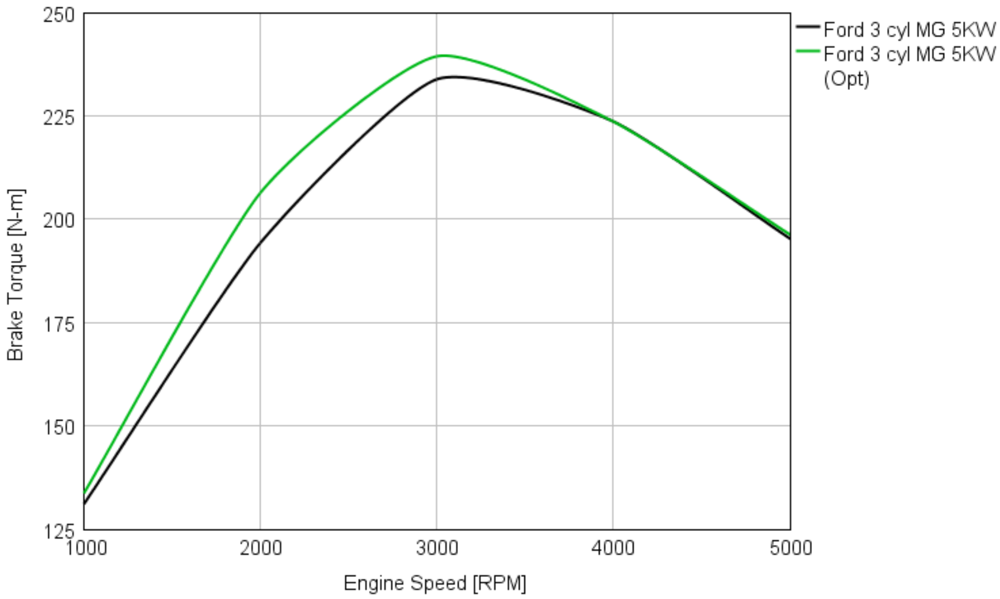

Figure 28: Brake Torque graphs for the initial (black) and optimised (green) EAT 5kW models.

In addition, the results in Figure 29 indicate that overall the brake specific fuel consumption (BSFC) of the engine model with the optimised compressor has been considerably reduced compared with the engine model with the initial compressor. Furthermore, the highest reduction in the brake specific fuel consumption BSFC of the electrically-assisted turbocharger (EAT) model occurred at low engine speed.

Moreover, Figure 30 outlines the average turbocharger shaft speed for the two engine models against time. Although the transient response time remained steady with the optimised compressor model, the maximum shaft speed has been increased by 3000 rpm as shown in Figure 28. Therefore, the overall performance of the engine model with the optimised compressor has been improved.

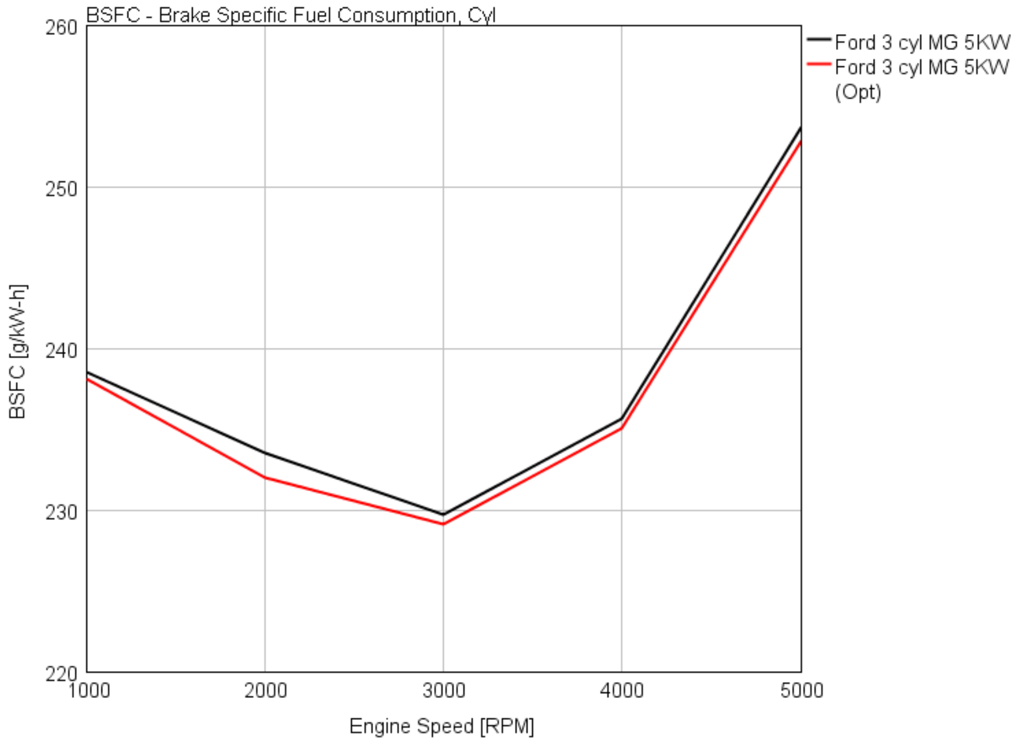

Figure 29: Brake specific fuel consumption (BSFC) graphs for the initial and optimized electrically-assisted turbocharger (EAT) 5kW models.

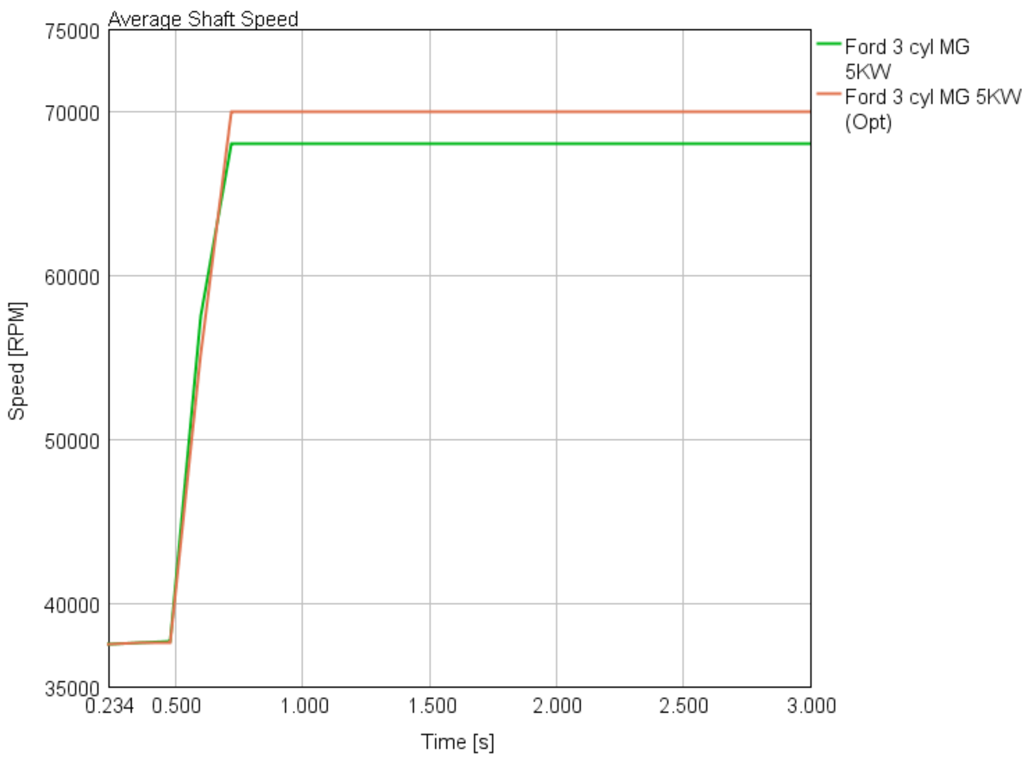

Figure 30: Average Shaft speed of the electrically-assisted turbocharger (EAT) models with 5kW power level at 1000 rpm engine speed.

7. Conclusion

A design methodology is implemented based on authoritative loss models for the preliminary design of a centrifugal electrically-assisted turbocharger (EAT) compressor. The methodology extended to engine performance modeling for a conventionally and an electrically-assisted turbocharger (EAT)-equipped engine layout. The calculated compressor geometry arising from the proposed method was imported to the engine simulation software while the EAT-equipped engine was tested at five different power levels from 1kW to 5kW.

The results obtained from the engine simulations indicated that the electrically-assisted turbocharger (EAT) engine model improved the overall performance of the engine compared to the baseline engine. Moreover, the electrically-assisted turbocharger (EAT) equipped engine power output with 1kW and 5kW electrically-assisted turbocharger (EAT) power levels was increased by an average of 5.96% and 15.4%, respectively, from 1000 to 3000 rpm engine speed compared to the baseline model.

As far as the BSFC is concerned for the electrically-assisted turbocharger (EAT) model for 1kW and 5kW, there was an overall fuel consumption decrease of 0.53% and 1.45% depending on engine operating conditions, respectively, compared to the initial baseline engine model.

Author Contributions: Nikolaos Xypolitas and Mamdouh Alshammari were the research students that conducted the detailed study and wrote the first draft of this paper. Apostolos Pesyridis conceived of the project, created the layout of the investigations, and checked the computational outcome of the resultant modelling effort and subsequent discussion.

Conflicts of Interest: The authors declare no conflict of interest.

Nomenclature

Variables

C_m	Meridional component of absolute velocity [m/s]
C_u	Tangential component of absolute velocity [m/s]
Cp	Specific heat at constant pressure [J/(kg·K)]
N	Rotational speed of turbocharger [rpm]
P	Pressure [bar]
R	Gas constant for air [J/(kg·K)]
r	Radius [mm]
T	Temperature [K]

Subscripts

0	Stagnation or total state; ambient condition
1-4	compressor stages
r	Radial velocity component
rms	Root mean square
Th	Throat parameter
Tr	Total relative

Greek letters

γ	Ratio of specific heats
Δ	Difference
ϱ	Density [kg/m^3]
$\bar{\varpi}$	Non-dimensional pressure loss

Acronyms

is, s isentropic
m Meridional velocity component

BMEP Brake mean effective pressure
BSFC Brake specific fuel consumption
EAT Electrically assisted turbocharger
MG Motor-Generator
RANS Reynolds Averaged Navier Stokes
rpm Revolution per minute

Nomenclature

Variables

C_m Meridional component of absolute velocity [m/s]
C_u Tangential component of absolute velocity [m/s]
Cp Specific heat at constant pressure [J/(kg·K)]
N Rotational speed of turbocharger [rpm]
P Pressure [bar]
R Gas constant for air [J/(kg·K)]
r Radius [mm]
T Temperature [K]

Subscripts

0 Stagnation or total state; ambient condition
1-4 compressor stages
is, s isentropic
m Meridional velocity component

r Radial velocity component
rms Root mean square
Th Throat parameter
Tr Total relative

Greek letters

γ Ratio of specific heats
Δ Difference
ϱ Density [kg/m^3]
$\bar{\omega}$ Non-dimensional pressure loss

Acronyms

BMEP Brake mean effective pressure
BSFC Brake specific fuel consumption
EAT Electrically assisted turbocharger
MG Motor-Generator
RANS Reynolds Averaged Navier Stokes
rpm Revolution per minute

References

1. Winterbone, D.E.; Benson, R.S.; Mortimer, A.G.; Kenyon, P.; Stotter, A. Transient Response of Turbocharged Diesel Engines. *Int. Automot. Eng. Congr. Expo., SAE International*;. doi:10.4271/770122.**1977**.
2. Pesiridis, A.; Ferrara, A.; Tuccillo, R.; Chen, H.;Conceptual design of an axial turbocharger turbine. *Proc ASME Turbo Expo*;8:1–12. doi:10.1115/GT2017-64825, **2017**.
3. Pesiridis, A.; Saccomanno, A.; Tuccillo, R.;Capobianco, A. Conceptual Design of a Variable Geometry, Axial Flow Turbocharger Turbine.*SAE Technical Paper* 2017-24-0163, **2017**.
4. Yang, M.Y.; Martinez-Botas, R.F.; Zhuge, W.L.; Qureshi, U., Richards, B.Centrifugal compressor design for electrically assisted boost.*IOP Conf Ser Mater Sci Eng*, 52, 2013. doi:10.1088/1757-899X/52/4/04, **2014**.

5. Grönman, A.; Sallinen, P.; Honkatukia, J.; Backman, J.; Uusitalo, A. Design and experiments of two-stage intercooled electrically assisted turbocharger.*Energy Convers Manag*, 111:115–24,. doi:10.1016/j.enconman.2015.12.055, **2016**.
6. Terdich, N.; Martinez-Botas, R.F.; Romagnoli, A.; Pesiridis, A. *Mild Hybridization Via Electrification of the Air System: Electrically Assisted and Variable Geometry Turbocharging Impact on an Off-Road Diesel Engine*. J Eng Gas Turbines Power;136:31703. doi:10.1115/1.4025887, **2013**.
7. Harley P, Spence S, Filsinger D, Dietrich M, Early J. *Experimental and Numerical Benchmarking of an Improved Meanline Modelling Method for Automotive Turbocharger Centrifugal Compressors*. ASME Turbo Expo 2015: Turbine Technical Conference and Exposition, Paper No. GT2015-42175, pp. V02CT42A008,Montreal, Quebec, Canada, June 15–19, **2015**.
8. Feneley, A, Pesiridis, A, and Chen, H. *A One-dimensional gas dynamics code for turbocharger pulsating flow and heat transfer performance modelling*. Conference Proceedings of ASME TURBO EXPO 2017, ASME GT2017-64743, Charlotte, USA, June 26-30, **2017**.
9. Rodgers, C.; Sapiro, L. Design Considerations for High-Pressure-Ratio Centrifugal Compressors, *ASME 1972 International Gas Turbine and Fluids Engineering Conference and Products Show*, Paper No. 72-GT-91, pp. V001T01A090, San Francisco, California, USA, March 26–30, **1972**.
10. Rajoo, S.; Romagnoli, A.; Martinez-Botas, R.; Pesiridis, A.; Copeland, C.; Mamat, A.M.I. Automotive Exhaust Waste Heat Recovery Technologies. In "Automotive Exhaust Emissions and Energy Recovery", *NOVA Science Publishers*, Hauppage, NY, USA, ISBN: 978-1-63321-493-4, **2014**.
11. Katrašnik, T.; Rodman, S.; Trenc, F.; Hribernik, A.; Medica, V. Improvement of the Dynamic Characteristic of an Automotive Engine by a Turbocharger Assisted by an Electric Motor. *J Eng Gas Turbines Power*, 125:590, **2003**.
12. Baines, N.C. Fundamentals of turbocharging. *Concepts NREC*, Vermont, USA, **2005**.
13. Harley, P.; Spence, S.; Filsinger, D.; Dietrich, M.; Early, J. Meanline Modeling of Inlet Recirculation in Automotive Turbocharger Centrifugal Compressors. *J. Turbomach* 137(1), 011007, **2014**.
14. Galvas, M.R. Fortran Program for Predicting Off-Design Performance of Centrifugal Compressors. *Report NASA-TN-D-7487*, E-7480, Washington D. C., **1973**.
15. Serrano, J.R.; Arnau, F.J.; García-Cuevas, L.M.; Dombrovsky, A.; Tartoussi, H. Development and validation of a radial turbine efficiency and mass flow model at design and off-design conditions. *Energy Convers Manag*, 128:281–93, **2016**.
16. Feneley, A.J.; Pesiridis, A.; Andwari, A.M. Variable Geometry Turbocharger Technologies for Exhaust Energy Recovery and Boosting-A Review. *Renew Sustain Energy* Rev, 71:959–75, **2017**.
17. Shah, S.V.; Vyas, B.G.; Bollavarapu, A.; Patel, S. Aerodynamic and Thermal Design of Centrifugal Compressor for Small Scale in Non-Dimemsional Form. *Int J Mech Prod Eng Res Dev*, 7:81–92, **2017**.
18. Johnston, J.P.; Dean, R.C.J. Losses in Vaneless Diffusers of Centrifugal Compressors and Pumps: Analysis, Experiment, and Design. *J Eng Power*, 88:49–60, **1966**.
19. Kerres, B.; Sanz, S.; Sundström, E.; Mihaescu, M.A Comparison of Performance Predictions between 1D Models and Numerical Data for a Turbocharger Compressor. *Proc. 12th Eur. Conf. Turbomach. Fluid Dyn. Thermodyn. ETC12*, April 3-7, Stock. Sweden , **2017**.
20. Aungier, R.H. Mean Streamline Aerodynamic Performance Analysis of Centrifugal Compressors. *J Turbomach*, 117:360–6, **1995**.
21. Oh, H.W.;, Yoon, E.S.; Chung, M.K. An optimum set of loss models for performance prediction of centrifugal compressors.*Proc Inst Mech Eng Part A J Power Energy* 211:331–8, **1997**.

22. Sundström, E.; Kerres, B.; Sanz, S.; Mihăescu, M. On the Assessment of Centrifugal Compressor Performance Parameters by Theoretical and Computational Models. V02CT44A029, **2017**.
23. Aungier, R.H. Centrifugal compressors: a strategy for aerodynamic design and analysis. New York: ASME Press; **2000**.
24. Japikse, D.; Baines, N.C. Introduction to turbomachinery. Norwich, Vt: *Concepts ETI*; **1994**.
25. Bathie, W.W. Fundamentals of gas turbines. New York: Wiley; **1984**.
26. Boyce, M.P. Centrifugal Compressors: A Basic Guide. Tulsa, Ok: Pennwell Books; **2003**.
27. Lee, B.K.; Ehsani, M. Advanced Simulation Model for Brushless DC Motor Drives. vol. 31. Taylor & Francis; **2003**.
28. Nishiwaki, K.; Iezawa, M.; Tanaka, H.; Goto, T., et al., "Development of High Speed Motor and Inverter for Electric Supercharger," SAE Technical Paper 2013-01-0931, **2013**.
29. Ford media. Available online: https://media.ford.com/content/dam/fordmedia/Europe/documents/productReleases/Focus/FordFocus_TechSpecs_EU.pdf (Accessed on 1 January 2018)